CMS Physics Analysis Summary

Contact: cms-phys-conveners-ftr@cern.ch 2018/11/21

Searches for light higgsino-like charginos and neutralinos at the HL-LHC with the Phase-2 CMS detector

The CMS Collaboration

Abstract

A search for the pair production of light higgsino-like charginos $\widetilde{\chi}_1^{\pm}$ and neutralinos $\widetilde{\chi}_2^0$ is presented, based on a simulation of 3000 fb^{-1} of proton-proton collision data produced by the HL-LHC at a center-of-mass energy of 14 TeV. The Phase-2 CMS detector is simulated using Delphes. The $\widetilde{\chi}_1^{\pm}$ and $\widetilde{\chi}_2^0$ are assumed to be mass-degenerate, to be pair-produced ($\widetilde{\chi}_1^{\pm}\widetilde{\chi}_2^0$, $\widetilde{\chi}_2^0\widetilde{\chi}_1^0$), and to decay into the lightest stable superymmetric particle $\widetilde{\chi}_1^0$ via off-shell W and Z bosons. The $\widetilde{\chi}_1^0$ is also assumed to be higgsino-like. Candidate signal events are required to have two same-flavor, opposite-charge, low transverse momentum leptons (electrons or muons), one jet, and significant missing transverse momentum.

1 Introduction

Supersymmetry (SUSY) [1–5] is considered one of the most compelling theories of physics beyond the standard model (SM). It postulates the existence of new particles with spin differing by half a unit with respect to that of their SM partners. The linear superposition of the fermionic partners of the Higgs and electroweak gauge bosons, the higgsinos and gauginos respectively, are referred to as charginos $\widetilde{\chi}^{\pm}_{1,2}$ and neutralinos $\widetilde{\chi}^{0}_{1,2,3,4}$. If R-parity [6] is conserved, the lightest supersymmetric particle (LSP) $\widetilde{\chi}^{0}_{1}$ is stable. The charginos and neutralinos are produced in pairs and decay into final states with SM particles and LSPs.

In scenarios of natural supersymmetry, the higgsinos may be the only low-mass supersymmetric states. The spectra will then be characterized by light higgsino-like $\widetilde{\chi}^{\pm}_{1}$, $\widetilde{\chi}^{0}_{2}$, and $\widetilde{\chi}^{0}_{1}$ particles, while all other sparticles exhibit masses above the TeV scale. A search for higgsino-like charginos and neutralinos is therefore critical to probe for natural SUSY at the LHC and the High-Luminosity LHC (HL-LHC).

If $\widetilde{\chi}^{\pm}_{1}$, $\widetilde{\chi}^{0}_{2}$, and $\widetilde{\chi}^{0}_{1}$ are higgsino-like, the mass splitting is driven by radiative corrections and acquires values up to a few GeV. As a result, pair-produced $\widetilde{\chi}^{\pm}_{1}\widetilde{\chi}^{0}_{2}$ or pair-produced $\widetilde{\chi}^{0}_{2}\widetilde{\chi}^{0}_{1}$ can decay promptly into $\widetilde{\chi}^{0}_{1}$ only via off-shell W and Z bosons, leading to events with low transverse momentum (p_{T}) SM particles. In leptonic decays of the Z boson, the events will contain one same-flavor, opposite-charge lepton pair, the invariant mass of which has a kinematic endpoint at $\Delta M(\widetilde{\chi}^{0}_{2},\widetilde{\chi}^{0}_{1}) = m(\widetilde{\chi}^{0}_{2}) - m(\widetilde{\chi}^{0}_{1})$. Sensitivity to the signal is achieved by requiring at least one jet from initial-state radiation (ISR) that recoils against the two $\widetilde{\chi}^{0}_{1}$ and produces significant missing transverse momentum ($p_{\mathrm{T}}^{\mathrm{miss}}$) in the event. Feynman diagrams for the signal processes are shown in Fig. 1. The ATLAS and CMS collaborations developed searches for higgsino-like $\widetilde{\chi}^{\pm}_{1}$ and $\widetilde{\chi}^{0}_{2}$ that used up to 36 fb^{-1} of proton-proton collision data [7, 8] and started probing the parameter space beyond the LEP experiments' limits [9, 10]. By providing 3000 fb^{-1} of proton-proton collision data at a center-of-mass energy of 14 TeV, the HL-LHC has the potential to significantly extend the experiments' sensitivity to higgsinos.

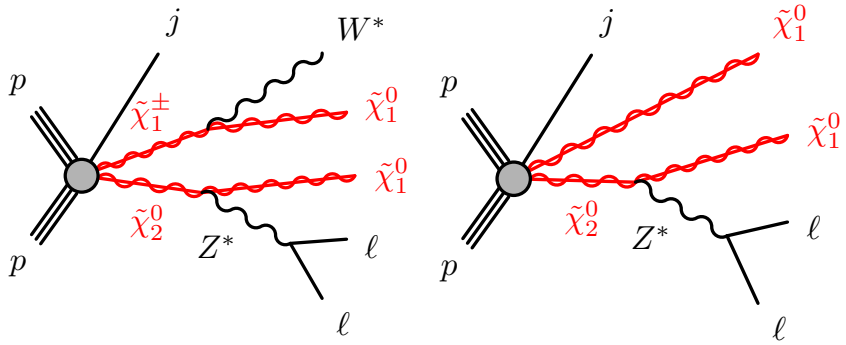

Figure 1: Example Feynman diagrams for $\widetilde{\chi}^{\pm}_{1}\widetilde{\chi}^{0}_{2}$ (left) and $\widetilde{\chi}^{0}_{2}\widetilde{\chi}^{0}_{1}$ (right) s-channel pair production, followed by the leptonic decay of the $\widetilde{\chi}^{0}_{2}$.

The model used for the optimization of the search and its interpretation is a SUSY simplified model [11] where the higgsino-like $\widetilde{\chi}^{\pm}_{1}$ and $\widetilde{\chi}^{0}_{2}$ are assumed to be mass-degenerate and produced in pairs. The model thus contains both the $\widetilde{\chi}^{\pm}_{1}\widetilde{\chi}^{0}_{2}$ and the $\widetilde{\chi}^{0}_{2}\widetilde{\chi}^{0}_{1}$ production, where $\widetilde{\chi}^{\pm}_{1}$ decays into $\mathrm{W}^{*}\widetilde{\chi}^{0}_{1}$ and $\widetilde{\chi}^{0}_{2}$ into $\mathrm{Z}^{*}\widetilde{\chi}^{0}_{1}$, respectively, with a branching fraction of 100%. The region of parameter space explored by this analysis includes $m_{\widetilde{\chi}^{\pm}_{1}} = m_{\widetilde{\chi}^{0}_{2}}$ larger than 100 GeV to account for the lower limit set by the LEP experiments, as well as $5.0 \leq \Delta M(\widetilde{\chi}^{0}_{2},\widetilde{\chi}^{0}_{1}) \leq 40$ GeV. The lower and upper bounds on $\Delta M(\widetilde{\chi}^{0}_{2},\widetilde{\chi}^{0}_{1})$ are driven by the minimum lepton p_{T} requirement, the suppression of background events containing low mass resonances such as J/ψ, and

the expected mass separation between the $\widetilde{\chi}_2^0$ and $\widetilde{\chi}_1^0$. In this region of parameter space, the $Z^* \to \ell\ell$ (ℓ = electron, muon) branching fraction depends only slightly on the $\widetilde{\chi}_2^0$ to $\widetilde{\chi}_1^0$ mass splitting (sub-percent impact); the branching fraction is therefore assumed to be the same as the branching fraction of the on-shell Z boson.

The cross sections are calculated for $\sqrt{s} = 14\,\text{TeV}$ at next-to-leading-order (NLO) plus next-to-leading-logarithmic (NLL) precision with the CTEQ 6.6 and MSTW 2008nlo90cl parton distribution functions (PDFs) using the RESUMMINO code [12, 13]. The signal samples are generated by the MADGRAPH5_aMC@NLO 2.2.2 [14] event generator up to two additional jets at leading order (LO) precision in perturbative QCD using the MLM merging scheme [15]. The supersymmetric particles are then decayed by the PYTHIA 8.212 package [16]. PYTHIA also provides parton showering and hadronization. The simplified models do not include any spin correlations in the decays. MADGRAPH5_aMC@NLO 2.2.2 is also used to produce selected parton-level background processes at LO (Drell-Yan, W+jets), with the parton showering and hadronization provided by PYTHIA. The W^+W^- events are generated at NLO precision using the FxFx merging scheme [17] and scaled to the NLO cross-section [18]. The NNPDF3.0 [19] LO and NLO PDFs are used for the simulated samples generated at LO and NLO, respectively. Only the $t\bar{t}$ events are generated using MADGRAPH5 v1.5.10 and the CTEQ 6l1 PDF set [20].

All background events, except for the pair production of top quarks and of W bosons, are generated at $\sqrt{s} = 13\,\text{TeV}$ and the corresponding cross sections are scaled to 14 TeV. The $t\bar{t}$ and the W^+W^- events are generated at a center-of-mass energy of 14 TeV. The effect of multiple interactions per bunch crossing (pileup) is estimated by overlaying the hard scatter event with minimum bias events drawn from a Poisson distribution with an average of 200.

The CMS detector [21] will be substantially upgraded in order to fully exploit the physics potential offered by the increase in luminosity at the HL-LHC [22], and to cope with the demanding operational conditions at the HL-LHC [23–27]. The upgrade of the first level hardware trigger (L1) will allow for an increase of L1 rate and latency to about 750 kHz and 12.5 μs, respectively, and the high-level software trigger is expected to reduce the rate by about a factor of 100 to 7.5 kHz. The entire pixel and strip tracker detectors will be replaced to increase the granularity, reduce the material budget in the tracking volume, improve the radiation hardness, extend the geometrical coverage, and provide efficient tracking up to pseudorapidities of about $|\eta| = 4$. The muon system will be enhanced by upgrading the electronics of the existing cathode strip chambers, resistive plate chambers (RPC), and drift tubes. New muon detectors based on improved RPC and gas electron multiplier technologies will be installed to add redundancy, increase the geometrical coverage up to about $|\eta| = 2.8$, and improve the trigger and reconstruction performance in the forward region. The barrel electromagnetic calorimeter will feature the upgraded front-end electronics that will be able to exploit the information from single crystals at the L1 trigger level, to accommodate trigger latency and bandwidth requirements, and to provide 160 MHz sampling allowing high precision timing capability for photons. The hadronic calorimeter, consisting in the barrel region of brass absorber plates and plastic scintillator layers, will be read out by silicon photomultipliers. The endcap electromagnetic and hadron calorimeters will be replaced with a new combined sampling calorimeter that will provide highly-segmented spatial information in both transverse and longitudinal directions, as well as high-precision timing information. Finally, the addition of a new timing detector for minimum ionizing particles in both barrel and endocap region is envisaged to provide capability for 4-dimensional reconstruction of interaction vertices that will allow to significantly offset the CMS performance degradation due to high pileup rates.

A detailed overview of the CMS detector upgrade program is presented in Refs. [23–27], while

the expected performance of the reconstruction algorithms and pileup mitigation with the CMS detector is summarised in Ref. [28].

The generated signal and background events are processed with the fast-simulation package Delphes [29] in order to simulate the expected response of the upgraded CMS detector. The object reconstruction and identification efficiencies, as well as the detector response and resolution, are parameterised in Delphes using the detailed simulation of the upgraded CMS detector based on the GEANT4 package [30, 31].

2 Event reconstruction

In this analysis, the particle-flow (PF) [32] algorithm is used to attempt to reconstruct and identify each individual particle in the event. The algorithm considers information from all CMS sub-detectors to provide a global event description. In addition, the "Pileup Per Particle Identification" (PUPPI) [33] algorithm calculates the likelihood that each particle originates from a pileup interaction.

The $\widetilde{\chi}_2^0$ is expected to decay into $\widetilde{\chi}_1^0$ by emitting a low-mass Z^* boson in the central region of the detector. Muons (electrons) are therefore selected with $5 \leq p_T \leq 30\,\text{GeV}$ and $|\eta| \leq 2.4\,(1.6)$. Dedicated identification criteria, including a requirement on the lepton impact parameter, are used to identify leptons. The identification efficiency for muons with p_T of 5 GeV is 40% over the considered $|\eta|$ interval, while it ranges from 90 to 70% for muons with p_T of 30 GeV. The efficiency for electrons with p_T of 5 GeV is between 25 and 20% as η increases from 0 to 1.6, and between 80 to 60% for electrons with p_T of 30 GeV. Once identified, muons and electrons are considered candidate leptons if the scalar sum of track momenta in a cone around the lepton is less than 5 GeV and smaller than 50% of the lepton p_T. The cone's radius is defined to be $R = \sqrt{\Delta\phi(\ell,\text{tk})^2 + \Delta\eta(\ell,\text{tk})^2} = 0.3$, where ℓ refers to the lepton and tk to the tracks within the cone, and ϕ is the azimuthal angle. For electrons, the energy in the isolation cone is computed using the PUPPI algorithm. The isolation efficiency increases from 65% to 90% as the lepton p_T increases from 5 to 30 GeV.

The anti-k_T algorithm [34] with a size parameter of 0.4, implemented in the FastJet program [35], is adopted to reconstruct jets. In this analysis, candidate jets are jets with $p_T > 40\,\text{GeV}$ GeV and $|\eta| \leq 4.0$. Candidate jets consistent with the decay and hadronization of a B hadron are tagged as b jets with an efficiency of 74% [36]. Candidate jets with $p_T > 200\,\text{GeV}$ and $|\eta| \leq 2.4$ are referred to as ISR jets.

Candidate leptons and jets are required to be separated in space by $\Delta R = \sqrt{\Delta\phi(\ell,j)^2 + \Delta\eta(\ell,j)^2}$ greater than 0.4. ΔR is computed for each combination of a candidate lepton (ℓ) and a jet (j).

The missing transverse momentum vector $\vec{p}_T^{\,\text{miss}}$ is defined as the negative vector sum of all PF objects in the event with their corresponding transverse momenta weighted through the PUPPI method. Its magnitude is referred to as p_T^{miss}.

3 Search strategy

This search targets the production of $\widetilde{\chi}_1^{\pm}\widetilde{\chi}_2^0$ and $\widetilde{\chi}_2^0\widetilde{\chi}_1^0$, followed by the decay of $\widetilde{\chi}_2^0$ into $\widetilde{\chi}_1^0$ via a low mass virtual Z boson. Events are therefore requested to contain at least two low-p_T, same-flavor, opposite-charge candidate leptons. In candidate signal events, the invariant mass of the candidate leptons will exhibit a kinematic end point at $m_{\ell_1,\ell_2} = \Delta M(\widetilde{\chi}_2^0, \widetilde{\chi}_1^0)$.

In this analysis, it is assumed that either a $p_{\mathrm{T}}^{\mathrm{miss}}$-based trigger reaching a plateau efficiency for $p_{\mathrm{T}}^{\mathrm{miss}} \geq 250\,\mathrm{GeV}$ (similar to that used in [8]) or a single jet trigger with $p_{\mathrm{T}} > 170\,\mathrm{GeV}$ [37] is adopted to select events. In order to ensure high trigger efficiency, the events are required to have $p_{\mathrm{T}}^{\mathrm{miss}} \geq 300\,\mathrm{GeV}$ and to contain at least one candidate ISR jet (j_{ISR}) with p_{T} larger than 200 GeV. The ISR jet boosts the $\widetilde{\chi}_1^{\pm}\widetilde{\chi}_2^0$ or $\widetilde{\chi}_2^0\widetilde{\chi}_1^0$ system so that the outgoing $\widetilde{\chi}_1^0$ particles are aligned, increasing the $p_{\mathrm{T}}^{\mathrm{miss}}$. To further exploit the boosted topology of the signal, events are accepted only if the $p_{\mathrm{T}}^{\mathrm{miss}}$ and the ISR candidate jet p_{T} satisfy $\Delta\phi(p_{\mathrm{T}}^{\mathrm{miss}}, p_{\mathrm{T}}(j_{\mathrm{ISR}})) \geq 2.0$. Since minor hadronic activity is expected from the electroweak production of $\widetilde{\chi}_1^{\pm}$ and $\widetilde{\chi}_2^0$, an upper bound of 4 is placed on the number of candidate jets N_{jet}.

Several SM processes lead to events containing two same-flavor, opposite-charge candidate leptons, one ISR jet, and significant $p_{\mathrm{T}}^{\mathrm{miss}}$. One background category consists of prompt processes, where both candidate leptons originate from the prompt decay of W and Z bosons. Another category is misclassified processes, where at least one of the two candidate leptons originates from a semi-leptonic decay of a B hadron, a photon conversion, a decay in flight, or a misidentified quark or gluon. The prompt background is dominated by Drell-Yan (DY), diboson, and $\mathrm{t\bar{t}}$ production where both W bosons decay leptonically. The DY contribution is suppressed by requiring significant $p_{\mathrm{T}}^{\mathrm{miss}}$, while rejecting events with at least one b jet reduces the $\mathrm{t\bar{t}}$ background. The dominant misclassified processes are W and $\mathrm{t\bar{t}}$ production where one candidate lepton originates from the W boson decay and an additional misclassified lepton is selected in the event. Rejecting events with at least one b jet reduces both contributions. To further suppress the background contamination, events are accepted only if the angular separation between the two candidate leptons satisfies $\Delta R(\ell_1, \ell_2) \leq 2.0$, as expected of collinear leptons emerging from the decay of a boosted Z^* boson. Events satisfying the criteria described above, which are summarized in Table 1, form the baseline signal region.

Table 1: Definition of the baseline signal region. In the table below, N_ℓ is the number of lepton candidates; $\Delta R(\ell_1, \ell_2)$ is the angular separation between the two candidate leptons in the ϕ, η space; $N_{\text{b-jet}}$ is the number of b jets; N_{jet} is the number of candidate jets (including any ISR jet reconstructed in the event); N_{ISR} is the number of ISR jets; $\Delta\phi(p_{\mathrm{T}}^{\mathrm{miss}}, p_{\mathrm{T}}(j_{\mathrm{ISR}}))$ is the azimuthal distance between the $p_{\mathrm{T}}^{\mathrm{miss}}$ vector and the j_{ISR} p_{T} vector; and m_{ℓ_1,ℓ_2} is the invariant mass of the two candidate leptons.

Observable	Requirement
N_ℓ	$= 2$ (same flavor, opposite charge)
$\Delta R(\ell_1, \ell_2)$	≤ 2.0
$N_{\text{b-jet}}$	$= 0$
N_{jet}	≤ 4
N_{ISR}	≥ 1
$p_{\mathrm{T}}^{\mathrm{miss}}$	$\geq 250\,\mathrm{GeV}$
$\Delta\phi(p_{\mathrm{T}}^{\mathrm{miss}}, p_{\mathrm{T}}(j_{\mathrm{ISR}}))$	≥ 2.0
m_{ℓ_1,ℓ_2}	[5, 40] GeV

Figure 2 shows the p_{T} distributions of the candidate leptons with the highest and second-highest p_{T} in events satisfying the baseline signal region selection. In the signal models, the mean of the lepton p_{T} is correlated to the $\Delta M(\widetilde{\chi}_2^0, \widetilde{\chi}_1^0)$ mass difference. The $p_{\mathrm{T}}^{\mathrm{miss}}$ and m_{ℓ_1,ℓ_2} distributions are presented in Fig. 3.

The missing transverse momentum, the invariant mass of the two candidate leptons, and the sub-leading lepton $p_{\mathrm{T}}(\ell_2)$ observables are found to provide the best discrimination between signal and background. Events in the baseline signal region are therefore classified in 60 cate-

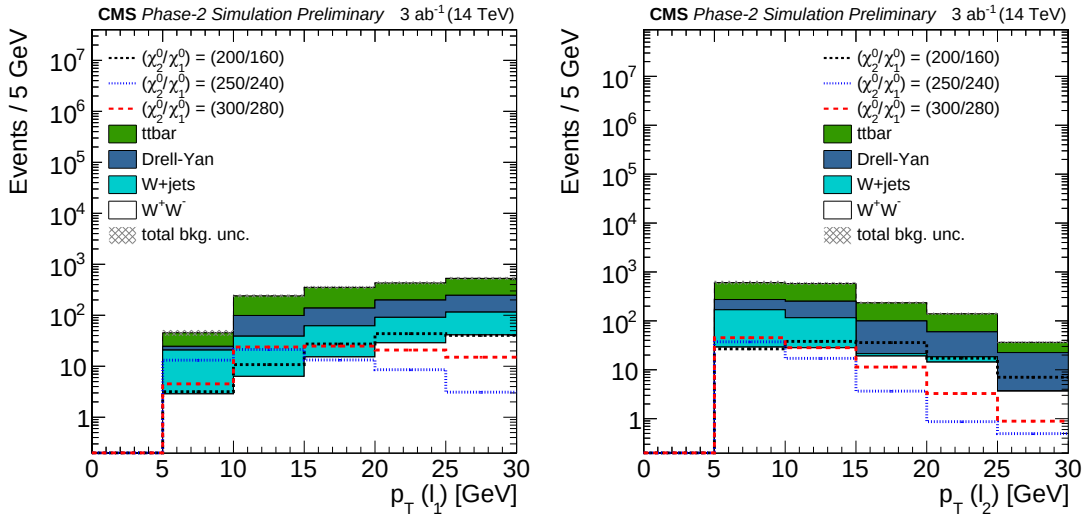

Figure 2: Distributions of the candidate lepton with the highest p_{T} (left) and the second-highest p_{T} (right) for background and signal events in the baseline signal region. Three selected $\widetilde{\chi}_1^{\pm}\widetilde{\chi}_2^0 + \widetilde{\chi}_2^0\widetilde{\chi}_1^0$ signal models are shown, where the first number corresponds to the mass of the $\widetilde{\chi}_2^0$ (and $\widetilde{\chi}_1^{\pm}$) and the second one to the mass of the $\widetilde{\chi}_1^0$. The uncertainty band represents systematical uncertainties.

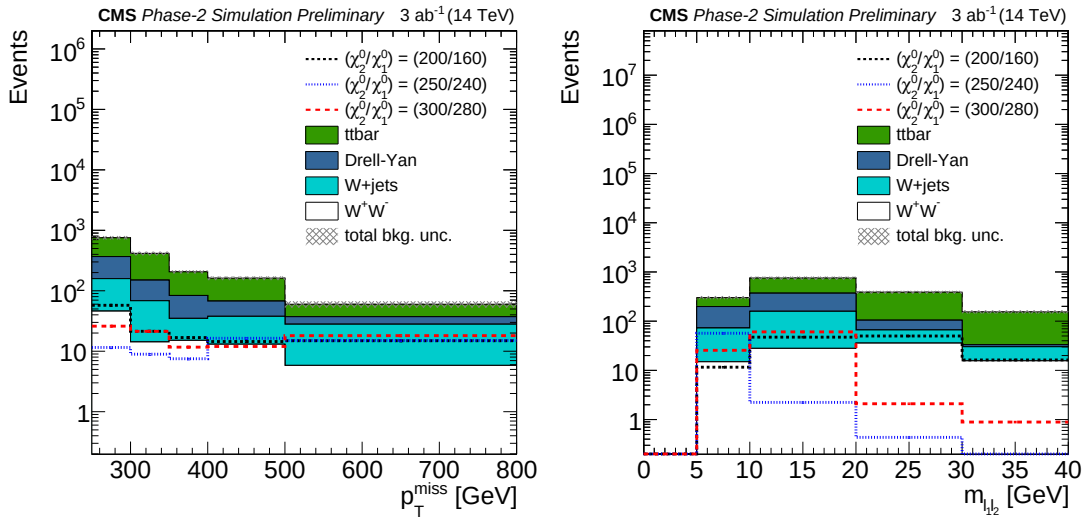

Figure 3: Distributions of the $p_{\mathrm{T}}^{\mathrm{miss}}$ (left) and m_{ℓ_1,ℓ_2} (right) for backgrund and signal events in the baseline signal region. Three selected $\widetilde{\chi}_1^{\pm}\widetilde{\chi}_2^0 + \widetilde{\chi}_2^0\widetilde{\chi}_1^0$ signal models are shown, where the first number corresponds to the mass of $\widetilde{\chi}_2^0$ (and $\widetilde{\chi}_1^{\pm}$) and the second one to the mass of $\widetilde{\chi}_1^0$. The uncertainty band represents systematical uncertainties.

gories with $p_{\mathrm{T}}^{\mathrm{miss}}$ values in [250, 300, 350, 400, 500, ∞] GeV, m_{ℓ_1,ℓ_2} values in [5, 10, 20, 30, 40] GeV, and $p_{\mathrm{T}}(\ell_2)$ in [5, 13, 21, 30] GeV. The categories are defined based on the $p_{\mathrm{T}}^{\mathrm{miss}}$ resolution and the expected kinematic endpoints of m_{ℓ_1,ℓ_2} and $p_{\mathrm{T}}(\ell_2)$ in the signal models.

The search approach in this analysis differs in several ways from the one adopted in the Run-2 analysis presented in Ref. [8]. In this analysis, facilitated by the large size of the dataset expected at the HL-LHC, substantially more signal regions are used. In turn, the baseline selection is loosened, with no dedicated requirements to suppress the $\mathrm{Z} \to \tau\tau$ background.

4 Expected sensitivity

There are several systematic uncertainties in the yields of both the background and the signal processes. The dominant experimental uncertainties are those originating from the jet energy corrections, b-tagging efficiency, lepton identification and isolation efficiency (combined in Table 2), and integrated luminosity. The uncertainties values are derived from those estimated in the current Run-2 based analyses with proper scaling to account for the larger dataset expected at the HL-LHC. These systematic uncertainties are correlated among the prompt background processes and between the signal and the prompt background yields. The uncertainty values are reported per source in Table 2. The uncertainty in the total background also includes the uncertainty in the determination of the misclassified component. This is assumed to be 30% based on the prediction in Ref. [8] that uses observed data. It is assumed that the yields are not affected by the statistical uncertainty due to the limited number of generated event.

Table 2: Summary of the experimental systematic uncertainties assumed in the prediction of the yields for processes with prompt leptons.

Source	Uncertainty
jet energy corrections	1–2.5%
b-tagging	1%
muon, electron efficiency	0.5, 2.5%
integrated luminosity	1%

Theoretical uncertainties in the cross sections and in the acceptance from the choice of parton distribution functions are considered negligible and are not included. However, a systematic uncertainty of 10% in the signal acceptance, similar to the value from Ref. [8], is included to account for the modeling of the ISR jet. The systematic uncertainties are treated as nuisance parameters with log-normal probability density functions.

The search sensitivity is calculated within the modified frequentist framework using the asymptotic formulae and the $\mathrm{CL_s}$ criterion to compute the results [38–40]. The upper limit on the cross sections is computed at 95% confidence level (CL) and shown in Fig. 4. These contours correspond to the combination of $\widetilde{\chi}_1^{\pm}\widetilde{\chi}_2^0$ and $\widetilde{\chi}_2^0\widetilde{\chi}_1^0$ production. The signal and background yields for two representative event categories (out of the total 60) that are sensitive to high-mass $\widetilde{\chi}_2^0$ signals are presented in Table 3. Higgsino-like mass-degenerate $\widetilde{\chi}_1^{\pm}$ and $\widetilde{\chi}_2^0$ are excluded for masses up to 360 GeV if the mass difference with respect to the lightest neutralino $\widetilde{\chi}_1^0$ is 15 GeV, extending the sensitivity achieved in Ref. [8] by $\approx$210 GeV. Fig. 4 also shows the 5σ discovery contour, computed using all signal regions without taking the look-elsewhere-effect into account. Under this assumption $\widetilde{\chi}_1^{\pm}$ and $\widetilde{\chi}_2^0$ can be discovered for masses as large as 250 GeV. These results demonstrate that the HL-LHC can significantly improve the sensitivity to natural SUSY.

Table 3: Signal and background yields in two representative event categories. SR1 is defined by $p_{\mathrm{T}}^{\mathrm{miss}} > 500\,\mathrm{GeV}$, m_{ℓ_1,ℓ_2} in [10, 20] GeV, and $p_{\mathrm{T}}(\ell_2)$ in [13, 21] GeV. SR2 is defined by $p_{\mathrm{T}}^{\mathrm{miss}} > 500\,\mathrm{GeV}$, m_{ℓ_1,ℓ_2} in [10, 20] GeV, and $p_{\mathrm{T}}(\ell_2)$ in [5, 13] GeV. The signal model considered here has $m_{\widetilde{\chi}_1^\pm} = m_{\widetilde{\chi}_2^0} = 300\,\mathrm{GeV}$ and $m_{\widetilde{\chi}_1^0} = 280\,\mathrm{GeV}$. Only systematic uncertainties are given.

Process	SR1	SR2
Signal	3.3 ± 0.2	8.9 ± 0.5
$\mathrm{t\bar{t}}$	1.7 ± 0.1	6.2 ± 0.6
W+jets	0.03 ± 0.01	15.8 ± 4.8
$\mathrm{W^+W^-}$	0.7 ± 0.04	1.5 ± 0.1
Drell-Yan	0.9 ± 0.1	1.9 ± 0.2

A potential improvement to the analysis is the addition of final states with three leptons originating from $\widetilde{\chi}_1^\pm \widetilde{\chi}_2^0 \to \ell\nu\widetilde{\chi}_1^0 \ell\ell\widetilde{\chi}_1^0$ decays. The acceptance can also be increased with lower requirements on the minimum lepton p_{T} or on the minimum m_{ℓ_1,ℓ_2}. The latter improvement is expected to increase the sensitivity to models with mass splittings below 7.5 GeV, provided that the background from low-mass resonances is suppressed.

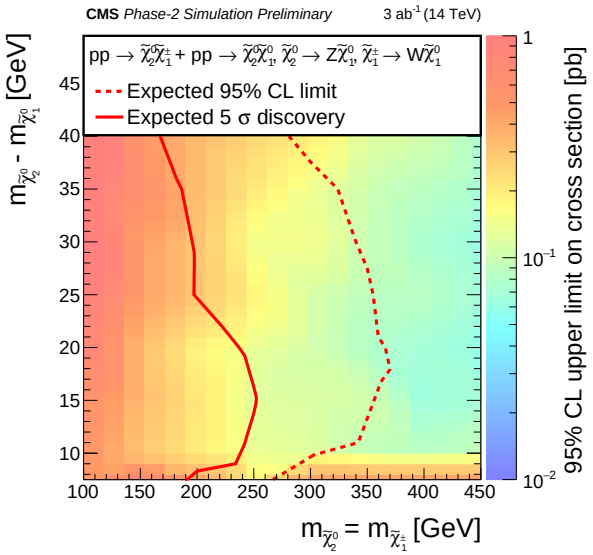

Figure 4: The 5σ discovery contours and expected 95% CL exclusion contours for the combined $\widetilde{\chi}_1^\pm\,\widetilde{\chi}_2^0$ and $\widetilde{\chi}_2^0\,\widetilde{\chi}_1^0$ production. Results are presented for $\Delta M(\widetilde{\chi}_2^0, \widetilde{\chi}_1^0) > 7.5$ GeV.

5 Summary

A search for the pair production of light higgsino-like charginos $\widetilde{\chi}_1^\pm$ and neutralinos $\widetilde{\chi}_2^0$ ($\widetilde{\chi}_1^\pm\widetilde{\chi}_2^0$, $\widetilde{\chi}_2^0\widetilde{\chi}_1^0$) is presented using $3000\,\mathrm{fb}^{-1}$ of simulated proton-proton collision data produced by the HL-LHC at 14 TeV. The $\widetilde{\chi}_1^\pm$ and $\widetilde{\chi}_2^0$ particles are assumed to be mass-degenerate, to be pair-produced, and to decay into the lightest stable superymmetric particle $\widetilde{\chi}_1^0$ via off-shell W and Z bosons. The $\widetilde{\chi}_1^0$ is also assumed to be higgsino-like. Higgsino-like mass-degenerate $\widetilde{\chi}_1^\pm$ and $\widetilde{\chi}_2^0$ particles with masses up to 250 GeV can be discovered for a mass difference of 15 GeV relative to the lightest neutralino $\widetilde{\chi}_1^0$. For this mass splitting, $\widetilde{\chi}_1^\pm$ and $\widetilde{\chi}_2^0$ with masses up to 360 GeV can be excluded at 95% confidence level.

References

[1] J. Wess and B. Zumino, "Supergauge transformations in four dimensions", *Nucl. Phys. B* (1974) 39, doi:10.1016/0550-3213(74)90355-1.

[2] H. P. Nilles, "Supersymmetry, supergravity and particle physics", *Phys. Rept.* **110** (1984) 1, doi:10.1016/0370-1573(84)90008-5.

[3] H. E. Haber and G. L. Kane, "The search for supersymmetry: Probing physics beyond the standard model", *Phys. Rept.* **117** (1985) 75, doi:10.1016/0370-1573(85)90051-1.

[4] R. Barbieri, S. Ferrara, and C. A. Savoy, "Gauge models with spontaneously broken local supersymmetry", *Nucl. Phys. B* (1982) 343, doi:10.1016/0370-2693(82)90685-2.

[5] S. Dawson, E. Eichten, and C. Quigg, "Search for supersymmetric particles in hadron-hadron collisions", *Nucl. Rev. D* **31** (1985) 1581, doi:10.1103/PhysRevD.31.1581.

[6] P. Fayet, "Supersymmetry and weak, electromagnetic and strong interactions", *Phys. Lett. B* **64** (1976) 159, doi:10.1016/0370-2693(76)90319-1.

[7] ATLAS Collaboration, "Search for electroweak production of supersymmetric states in scenarios with compressed mass spectra at $\sqrt{s}$ = 13 TeV with the ATLAS detector", *Phys. Rev. D* **97** (2018) 052010, doi:10.1103/PhysRevD.97.052010, arXiv:1712.08119.

[8] CMS Collaboration, "Search for new physics in events with two low momentum opposite-sign leptons and missing transverse energy at $\sqrt{s} = 13$ TeV", *Phys. Lett. B* **782** (2018) 440, doi:10.1016/j.physletb.2018.05.062, arXiv:1801.01846.

[9] ALEPH Collaboration, "Search for charginos nearly mass degenerate with the lightest neutralino in e^+e^- collisions at center-of-mass energies up to 209 GeV", *Phys. Lett. B* **533** (2002) 223, doi:10.1016/S0370-2693(02)01584-8, arXiv:0203020.

[10] DELPHI Collaboration, "Searches for supersymmetric particles in e^+e^- collisions up to 208 GeV and interpretation of the results within the MSSM", *Eur. Phys. J. C* **31** (2003) 421, doi:10.1140/epjc/s2003-01355-5, arXiv:0311019.

[11] D. Alves et al., "Simplified Models for LHC New Physics Searches", *J. Phys. G* **39** (2012) 421, doi:10.1088/0954-3899/39/10/105005, arXiv:1105.2838.

[12] B. Fuks, M. Klasen, D. R. Lamprea, and M. Rothering, "Gaugino production in proton-proton collisions at a center-of-mass energy of 8 TeV", *JHEP* **10** (2012) 081, doi:10.1007/JHEP10(2012)081, arXiv:1207.2159.

[13] B. Fuks, M. Klasen, D. R. Lamprea, and M. Rothering, "Precision predictions for electroweak superpartner production at hadron colliders with RESUMMINO", *Eur. Phys. J. C* **73** (2013) 2480, doi:10.1140/epjc/s10052-013-2480-0, arXiv:1304.0790.

[14] J. Alwall et al., "The automated computation of tree-level and next-to-leading order differential cross sections, and their matching to parton shower simulations", *JHEP* **07** (2014) 079, doi:10.1007/JHEP07(2014)079, arXiv:1405.0301.

[15] J. Alwall et al., "Comparative study of various algorithms for the merging of parton showers and matrix elements in hadronic collisions", *Eur. Phys. J. C* **53** (2008) 473, doi:d10.1140/epjc/s10052-007-0490-5, arXiv:0706.2569.

[16] T. Sjöstrand et al., "An introduction to PYTHIA 8.2", *Comput. Phys. Commun.* **191** (2015) 159, doi:10.1016/j.cpc.2015.01.024, arXiv:1410.3012.

[17] R. Frederix and S. Frixione, "Merging meets matching in MC@NLO", *JHEP* **12** (2012) 61, doi:10.1007/JHEP12(2012)061, arXiv:1209.6215.

[18] T. Gehrmann et al., "W^+W^- Production at Hadron Colliders in NNLO QCD", *Phys. Rev. Lett.* **113** (2014) 212001, doi:10.1103/PhysRevLett.113.212001, arXiv:1408.5243.

[19] NNPDF Collaboration, "Parton distributions for the LHC Run II", *JHEP* **04** (2015) 040, doi:10.1007/JHEP04(2015)040, arXiv:1410.8849.

[20] A. Avetisyan et al., "Methods and Results for Standard Model Event Generation at 14 TeV, 33 TeV and 100 TeV Proton Colliders: A Snowmass Whitepaper", (2013). arXiv:1308.1636.

[21] CMS Collaboration, "The CMS Experiment at the CERN LHC", *JINST* **3** (2008) S08004, doi:10.1088/1748-0221/3/08/S08004.

[22] G. Apollinari et al., "High-Luminosity Large Hadron Collider (HL-LHC) : Preliminary Design Report", doi:10.5170/CERN-2015-005.

[23] CMS Collaboration, "Technical Proposal for the Phase-II Upgrade of the Compact Muon Solenoid", CMS Technical Proposal CERN-LHCC-2015-010, CMS-TDR-15-02, CERN, 2015.

[24] CMS Collaboration, "The Phase-2 Upgrade of the CMS Tracker", CMS Technical Design Report CERN-LHCC-2017-009, CMS-TDR-014, CERN, 2017.

[25] CMS Collaboration, "The Phase-2 Upgrade of the CMS Barrel Calorimeter", CMS Technical Design Report CERN-LHCC-2017-011, CMS-TDR-015, CERN, 2017.

[26] CMS Collaboration, "The Phase-2 Upgrade of the CMS Endcap Calorimeter", CMS Technical Design Report CERN-LHCC-2017-023, CMS-TDR-019, CERN, 2017.

[27] CMS Collaboration, "The Phase-2 Upgrade of the CMS Muon Detectors", CMS Technical Design Report CERN-LHCC-2017-012, CMS-TDR-016, CERN, 2017.

[28] CMS Collaboration, "CMS Phase-2 Object Performance", CMS Physics Analysis Summary, CERN, in preparation.

[29] DELPHES 3 Collaboration, "DELPHES 3, A modular framework for fast simulation of a generic collider experiment", *JHEP* **02** (2014) 057, doi:10.1007/JHEP02(2014)057, arXiv:1307.6346.

[30] GEANT4 Collaboration, "GEANT4: A Simulation toolkit", *Nucl. Instrum. Meth.* **A 506** (2003) 250, doi:10.1016/S0168-9002(03)01368-8.

[31] J. Allison et al., "Geant4 developments and applications", *IEEE Trans. Nucl. Sci.* **53** (2006) 270, doi:10.1109/TNS.2006.869826.

[32] CMS Collaboration, "Particle-flow reconstruction and global event description with the CMS detector", *JINST* **12** (2017) P10003, doi:10.1088/1748-0221/12/10/P10003, arXiv:1706.04965.

[33] D. Bertolini, P. Harris, M. Low, and N. Tran, "Pileup Per Particle Identification", *JHEP* **59** (2014) 1410, doi:10.1007/JHEP10(2014)059, arXiv:1407.6013.

[34] M. Cacciari, G. P. Salam, and G. Soyez, "The anti-k_t jet clustering algorithm", *JHEP* **04** (2008) 063, doi:10.1088/1126-6708/2008/04/063, arXiv:0802.1189.

[35] M. Cacciari, G. P. Salam, and G. Soyez, "FastJet user manual", *Eur. Phys. J. C* **72** (2012) 1896, doi:10.1140/epjc/s10052-012-1896-2, arXiv:1111.6097.

[36] CMS Collaboration, "Identification of heavy-flavour jets with the CMS detector in pp collisions at 13 TeV", *JINST* **13** (2018) P05011, doi:10.1088/1748-0221/13/05/P05011, arXiv:1712.07158.

[37] CMS Collaboration, "The Phase-2 Upgrade of the CMS L1 Trigger Interim Technical Design Report", CMS Technical Design Report CERN-LHCC-2017-013, CMS-TDR-017, CERN, 2017.

[38] G. Cowan, K. Cranmer, E. Gross, and O. Vitells, "Asymptotic formulae for likelihood-based tests of new physics", *Eur. Phys. J. C* **73** (2013) 2501, doi:10.1140/epjc/s10052-013-2501-z, arXiv:1007.1727.

[39] T. Junk, "Confidence level computation for combining searches with small statistics", *Nucl. Instr. Meth. A* **434** (1999) 435, doi:10.1016/S0168-9002(99)00498-2.

[40] A. L. Read, "Presentation of search results: the CLs technique", *J. Phys. G* **28** (2002) 2693, doi:10.1088/0954-3899/28/10/313.